Journal of Zhejiang University-SCIENCE A (Applied Physics & Engineering)
ISSN 1673-565X (Print); ISSN 1862-1775 (Online)
www.jzus.zju.edu.cn; www.springerlink.com
E-mail: jzus@zju.edu.cn

Influence of wet-dry cycles on vertical cutoff walls made of reactive magnesia-slag-bentonite-soil mixtures*

Hao-liang WU[1,2], Fei JIN[3], Yan-jun DU[†‡1]

[1]*Jiangsu Key Laboratory of Urban Underground Engineering & Environmental Safety, Institute of Geotechnical Engineering, Southeast University, Nanjing 210096, China*

[2]*Department of Civil and Environmental Engineering, Hong Kong University of Science and Technology, Hong Kong, China*

[3]*School of Engineering, University of Glasgow, Glasgow G12 8QQ, UK*

[†]E-mail: duyanjun@seu.edu.cn

Received June 30, 2019; Revision accepted Oct. 23, 2019; Crosschecked Nov. 7, 2019

Abstract: The strength and hydraulic conductivity of vertical cutoff walls consisting of reactive magnesia-activated ground granulated blast furnace slag (GGBS), bentonite, and soil (MSB) have been investigated in previous studies. However, there has been little comprehensive study of the influence of wet-dry cycles on the mechanical and microstructural properties of MSB backfills. In this paper, the durability of MSB backfills when exposed to wet-dry cycles is investigated. The variations in mass change, dry density, pH value, pore size distribution, and mineralogy are discussed. The results show that the mass change of ordinary Portland cement (OPC)-based and MSB backfills increases with respect to wet-dry cycles. The MSB backfills exhibit up to 8.2% higher mass change than OPC-based ones after 10 wet-dry cycles. The dry density, pH value, and unconfined compressive strength of MSB backfill decrease with the increasing number of wet-dry cycles. Increasing the GGBS-MgO content from 5% to 10% in MSB backfills results in 2.1–2.3 times higher strength, corresponding to a reduction of 2%–12% in cumulative pore volume; while increasing the bentonite content slightly reduces the strength of MSB mixtures, corresponding to an increase of cumulative pore volume by 4.6%–7.9%. The hydrotalcite-like phases and calcium silicate hydrate (C-S-H) are the primary hydration products in MSB backfills. Moreover, the continuous wet-dry cycles result in the precipitation of calcite and nesquehonite.

Key words: Cutoff wall; Reactive MgO-activated ground granulated blast furnace slag (GGBS); Durability; Wet-dry cycles; Carbonation

https://doi.org/10.1631/jzus.A1900300 **CLC number:** TU45

1 Introduction

The soil-cement-bentonite (SCB) cutoff wall has been widely used worldwide in remediation projects for contaminated sites (Ryan and Day, 2002; Opdyke and Evans, 2005; Ruffing and Evans, 2014). Such walls have been mainly used to interrupt the pollution pathway and to isolate the contaminant sourced from a vulnerable receptor (Joshi et al., 2008; Soga et al., 2013; Du et al., 2015; Wu et al., 2016; Li et al., 2018; Yang et al., 2018a, 2018b, 2019; Zhang et al., 2019). As compared to soil-bentonite (SB) and cement-bentonite (CB) cutoff walls, SCB walls possess adequate strength to carry foundation loads. They have the additional economic merit of the reuse of site-excavated soils (Ryan and Day, 2002; Opdyke and Evans, 2005). In CB and SCB walls, ordinary Portland cement (OPC) is the primary cementitious material used, and is associated with intensive CO_2

‡ Corresponding author

* Project supported by the National Key Research and Development Program (Nos. 2018YFC1803100 and 2018YFC1802300), the National Natural Science Foundation of China (No. 41877248), and the Primary Research & Development Plan of Jiangsu Province (No. BE2017715), China

ORCID: Hao-liang WU, https://orcid.org/0000-0002-2580-6719; Fei JIN, https://orcid.org/0000-0003-0899-7063

emissions (0.95 t/t OPC) and consumption of raw materials (Benhelal et al., 2013). In recent years, many industrial by-products such as ground granulated blast furnace slag (GGBS) and fly ash have become popular as partial substitutions for OPC in geotechnical applications (Jefferis, 2012; Arulrajah et al., 2017a, 2017b; Lam and Jefferis, 2017; Wu et al., 2019). For example, replacing OPC with GGBS in the cutoff wall backfill has been applied extensively in the UK (Jefferis, 2012). It has significant environmental and economic benefits, marginally affects the strength (sometimes with enhancement), slightly decreases pore water pH, and notably decreases hydraulic conductivity in the long term (Wu et al., 2019).

Compared to OPC, using reactive MgO as the activator for GGBS has many potential technical benefits, in particular for soil remediation applications. The main hydration products in reactive MgO-activated GGBS are calcium silicate hydrate (C-S-H), hydrotalcite, and brucite ($Mg(OH)_2$, if MgO is excessive) (Jin and Al-Tabbaa, 2014a; Yi et al., 2014; Jin et al., 2015; Du et al., 2016 ; Wang et al., 2016). Due to the absence of highly soluble portlandite with a high equilibrium pH value (~12.5) and the formation of the above-mentioned products with excellent adsorptive capacities, MgO-GGBS blends have shown superiority over OPC for contaminant immobilization in a number of laboratory studies and field trials (Jin and Al-Tabbaa, 2014a; Jin et al., 2014, 2015; Wang et al., 2016; Du et al., 2019).

Recently, this novel cement has been applied to form an innovative cutoff wall backfill material, together with bentonite and site sandy soil (Wu et al., 2019). The unconfined compressive strength (q_u) and hydraulic conductivity (k_w) of the proposed backfill permeated with tap water are in the ranges of 230–520 kPa and 1.1×10^{-10}–6.3×10^{-10} m/s at 90-d curing, respectively, complying well with the commonly adopted design limits ($q_u\geq100$ kPa and $k_w\leq1.0\times10^{-8}$ m/s) (ICE, 1999; Ryan and Day, 2002). More importantly, this backfill showed excellent durability under exposure to sodium sulfate (Na_2SO_4) or lead-zinc (Pb-Zn) solutions (Wu et al., 2019). Environmental and cost assessments demonstrated that this innovative magnesia-activated slag-bentonite (MSB) backfill material reduced CO_2 emissions by 85% with 15.3%–16.9% lower cost when compared with OPC-based SCB backfills.

In a scenario of cutoff wall installations, the groundwater levels at each side of the barrier may fluctuate over time (Evans, 1991; Ross and Beljin, 1998). The potential changes in the q_u and k_w of the cutoff wall exposed to cyclic wet-dry actions have been recognized as a medium- to long-term performance concern (National Research Council, 2007; Malusis et al., 2011; Soga et al., 2013). For CB and SCB walls, noticeable cracks were observed due to shrinkage in the drying phase (Soga et al., 2013), which would lead to the increase of k_w by 2–3 orders (Joshi et al., 2010). Previous studies also illustrated that the q_u of MgO-GGBS stabilized kaolin clay reduced dramatically with increasing wet-dry cycles (Du et al., 2016). Thus, it is necessary to evaluate the durability of the innovative MSB backfill under wet-dry cycles.

This paper aims to investigate the effect of wet-dry cycles on the durability of innovative MSB backfill. A series of laboratory tests, including mass change, dry density, pH value, unconfined compression tests, mercury intrusion porosimetry (MIP), and X-ray diffraction (XRD) are performed in order to reveal the effects of wet-dry cycles on the properties of MSB backfills.

2 Materials and specimen preparation

2.1 Solid materials

The backfill materials were prepared using Nanjing local soil, powdered sodium activated calcium-bentonite, MgO, and GGBS. The Nanjing local soil is classified as clayey sand based on the unified soil classification system (ASTM, 2017). The commercial powdered sodium activated calcium-bentonite was provided by the Mufeng Mineral Processing Plant in Zhenjiang, China. GGBS and MgO used in this study were obtained from Nanjing and Jinan, China, respectively. The physicochemical properties for the site soil and bentonite are shown in Table 1. The moisture, liquid and plastic limit, and specific gravity were measured according to ASTM D2216 (ASTM, 2010a), ASTM D854 (ASTM, 2014), and ASTM D4318 (ASTM, 2010b), respectively. The pH was measured by ASTM D4972 (ASTM, 2018a) using a pH meter HORIBAD-54. The cation exchange capacity was measured as in ASTM D7503

(ASTM, 2010d). The specific surface area was measured by nitrogen adsorption using a physisorption analyzer ASAP2020 according to Cerato and Lutenegger (2002). The medium reactivity MgO (reactivity is 102 s, determined by the acetic acid test according to Shand (2006)) was selected due to its appropriate reactivity and cost (Jin and Al-Tabbaa, 2014b; Wu et al., 2018a, 2018b). The chemical compositions of the soil, GGBS, and MgO used for this study are shown in Table 2 (Wu et al., 2019), as measured by X-ray fluorescence (XRF) (ARL™ SMS-2000).

Table 1 Physicochemical properties of materials

Index	Value			
	Clayey sand	Bentonite	GGBS	MgO
Moisture (%)	4.81	11.20	–	–
pH	7.32	8.60	10.96	10.53
Specific gravity, G_s	2.62	2.66	–	–
Plastic limit, w_P (%)	–	55	–	–
Liquid limit, w_L (%)	–	103	–	–
Grain size distribution (%)				
Clay (<0.002 mm) [a]	5.62	99.00	–	–
Silt (0.002–0.075 mm) [a]	14.18	1.00	–	–
Sand (0.075–2 mm) [b]	80.20	–	–	–
Specific surface area, SSA (m^2/g)	–	378.50	0.29	28.02
Exchangeable cation (cmol/kg)				
Ca^{2+}		22.74		
Mg^{2+}		1.41		
Na^+		53.39		
K^+		0.53		
Sum		78.07		

[a] Measured using a laser particle analyzer Mastersizer 2000 (Malvern Instruments Ltd., UK); [b] Measured with standard #10–#200 sieves

Table 2 Chemical compositions of the materials used in this study determined by XRF (Wu et al., 2019)

Oxide	Chemical composition (in weight) (%)		
	OPC	GGBS	MgO
CaO	49.75	34.00	0.23
Al_2O_3	10.87	17.90	0.28
MgO	2.26	6.02	92.95
K_2O	0.75	0.64	0.01
SiO_2	22.60	34.30	0.28
Fe_2O_3	3.50	1.02	–
SO_3	3.84	1.64	0.45
MnO	0.24	0.28	0.01
Loss of ignition (%)	6.19	4.20	5.79

2.2 Backfill mix design and specimen preparation

Table 3 shows the mix proportions of the studied backfills. The MgO to GGBS ratio was 1:9 to achieve good strength and the lowest hydraulic conductivity based on preliminary studies (Jin et al., 2015; Wu et al., 2018a, 2019). The binder (OPC or GGBS-MgO) dosages (by weight of dry soil) ranged from 2.5% to 12.5% based on a review of previous studies (Fig. 1) as reported by Wu et al. (2019), which included both field and lab test results of SCB cutoff walls. Furthermore, since natural high-quality Na-bentonite in China is scarce, in practice engineers usually prefer to choose a higher dosage (≥5%) of sodium activated calcium-bentonite. The raw solid materials, including the clayey sand, powdered sodium activated calcium-bentonite, OPC or MgO, and GGBS were weighed and mixed in a 2-L Hobart stainless steel mixer at 30 r/min for 5 min. It should be noted that the backfill specimens were prepared by mixing the non-prehydrated bentonite with sandy soil-OPC or sandy soil-GGBS-MgO mixture. Then, the predetermined amount of tap water (pH=6.8, electronic conductivity (EC)=3.3 μS/cm) was added and mixed at 60 r/min for 10 min to achieve homogeneity with the same slump value ((150±5) mm) (Wu et al., 2019). In the OPC-based backfill, the content of the GGBS used in this study was 80% replacement of OPC, which was reported to exhibit the lowest k_w and the highest q_u (Opdyke and Evans, 2005). The mixtures were

Table 3 Mix design for the backfills used in this study (Wu et al., 2019)

Backfill code	Proportion (in weight according to clayey sand) (%)			
	Bentonite	OPC	GGBS	MgO
C5	–	5	–	–
C5B5	5	5	–	–
C10B10	10	10	–	–
CS5B5	5	1	4.0	–
CS10B10	10	2	8.0	–
MS5B5	5	–	4.5	0.5
MS5B10	10	–	4.5	0.5
MS5B15	15	–	4.5	0.5
MS10B10	10	–	9.0	1.0
MS10B15	15	–	9.0	1.0

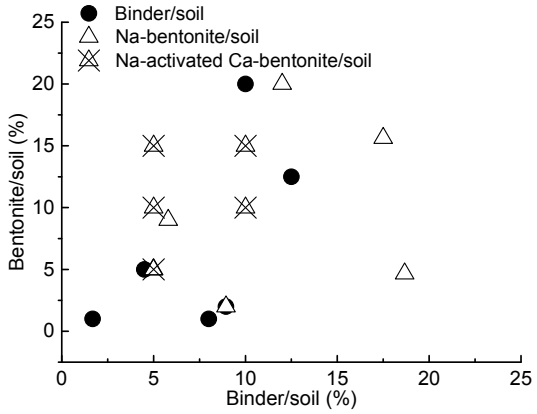

Fig. 1 Summary of bentonite/soil and binder/soil ratios in SCB cutoff wall backfill mix designs reported in (Wu et al., 2019)

poured into cylindrical moulds with sizes of 50 mm (diameter)×100 mm (height) and cured for 90 d under standard curing conditions (T=(20±2) °C, relative humidity (RH)=95%).

3 Materials and specimen preparation

The 90-d cured specimens were subjected to wet-dry cycles according to Kamon et al. (1993). For each drying cycle, the specimens were stored in an oven (30 °C) for 48 h, followed by soaking in the distilled water with a temperature of 20 °C for 24 h. The drying temperature was set as 30 °C to represent the typical average temperature of hot seasons in the southeast regions of China and to minimize the effect of accelerated slag hydration due to temperature rise (Du et al., 2016). The duration of such a wet-dry cycle was 3 d and it was repeated for 10 cycles.

After the ith wet or dry cycle, the mass change (MC) of the specimen is calculated by

$$\mathrm{MC}=(m_0-m_i)/m_0, \tag{1}$$

where m_0 is the initial mass of the specimen measured prior to the wet-dry cycles, and m_i is the mass of the sample measured immediately after the ith drying cycle.

The densities of the specimens were measured in triplicate as in ASTM D7263 (ASTM, 2018b), and average values were reported. The specimens were subjected to unconfined compressive test as in ASTM D4219 (ASTM, 2008) with a strain rate of 1%/min. Fragments from the core of the broken unconfined compressive test specimens were air-dried, crushed, and passed through a 2-mm sieve. Ten grams of the sieved soil and 10 mL of distilled water (water to solid ratio is 1:1) were poured into a glass container to determine the pore water pH. The pH values of the supernatant were measured by a HORIBA D-54 pH meter and the average value was reported.

After the 10th wet-dry cycle, dry specimens were prepared to conduct MIP and XRD tests. Briefly, ~1 cm^3 sample was collected from the specimen's core by a stainless steel knife and frozen in liquid nitrogen. The frozen sample was dried in a vacuum chamber at −80 °C. The MIP tests were conducted according to ASTM D4404 (ASTM, 2010c) using an Auto Pore IV 9510 mercury intrusion porosimeter to determine the pore size distribution. Prior to XRD analysis, the dry specimens were ground and sieved to <0.075 mm. The XRD spectra were obtained using a RigakuD/Max-2500 spectrometer using a Cu-Kα source with a wavelength of 0.15405 nm. The instrument was operated at 40 kV and 20 mA. A step size of 2θ=0.02° and a scanning speed of 5 s/step were used over a range from 10° to 50° in the step scan mode.

4 Results and discussion

4.1 Mass change and visual inspection of physical integrity

Figs. 2a and 2b present the variations in mass change with the wet-dry cycles for the OPC-based and MSB backfills. It can be seen that the mass changes of the two types of backfill increase with respect to the wet-dry cycles. Increasing the binder content (GGBS-MgO) in the MSB backfills reduces mass change (by ~9.0%–11.0%) (i.e. comparing MS10B10 and MS10B15 with MS5B10 and MS5B15, respectively). Fig. 2b also indicates that increasing the bentonite content from 5% to 15% leads to a higher mass change for the MSB backfills. This is attributed to the fact that higher bentonite content (i.e. MS5B15) is more sensitive to the loss of water as compared to MS5B5 and MS5B10, which

would develop matrix suction and increase the shrinkage in the backfills in the drying stages (Nahlawi and Kodikara, 2006; Rowe et al., 2011; Tang et al., 2011). However, the binder and bentonite contents show no significant impact on the OPC-based backfills as shown in Fig. 2a.

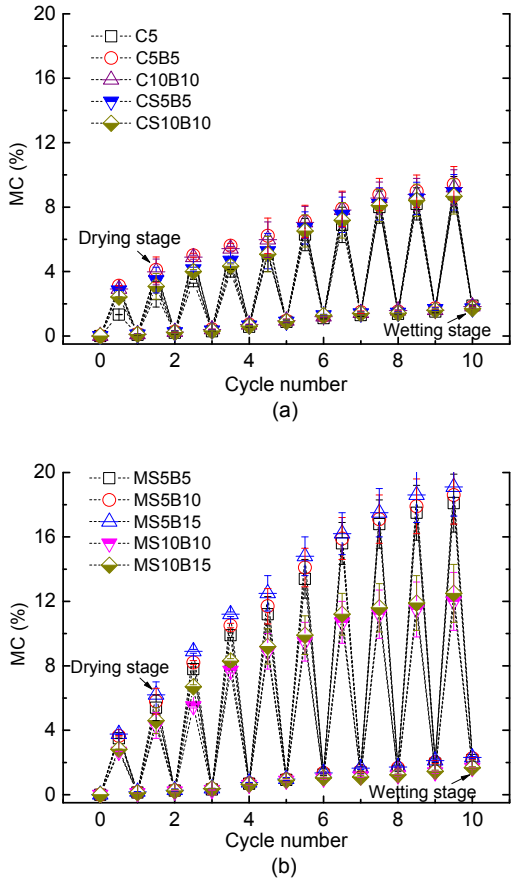

Fig. 2 Variations in mass change with wet-dry cycles for OPC-based backfills (a) and MSB backfills (b)

After the last wet-dry cycle, the mass changes in MSB backfills reach approximately 12%–19%, and are slightly higher than those for the OPC-based backfills. Meanwhile, the mass change is much higher in MSB than OPC at the wetting stage; the difference is much smaller at the drying stage. This may imply that the water absorption potential of the bentonite in MSB mixtures is better preserved than that in OPC-based mixtures. It was also found that spalling and macro-cracks started to develop at the 4th–6th cycles and were exacerbated with each wet-dry cycle, as shown in Fig. 3.

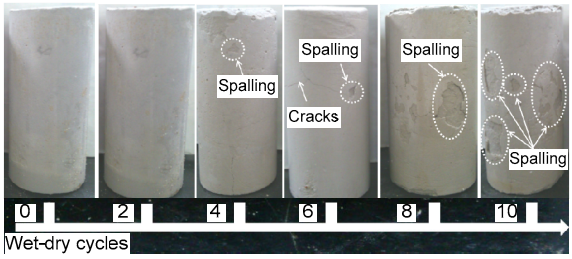

Fig. 3 Photos showing the physical integrity of MSB backfills during wet-dry cycling

4.2 Dry density

Fig. 4 shows the variations of average values and standard deviations (STDs) of dry densities with wet-dry cycles for OPC-based and MSB backfills. The dry densities of OPC-based and MSB backfills are 1.34–1.39 g/cm^3 and 1.31–1.35 g/cm^3 after the 10th wet-dry cycles, respectively. For all backfills, the dry density decreases slightly with the wet-dry cycles, which is consistent with the mass change evolution as shown in Fig. 2. For the identical binder and bentonite content, it is found that the dry density of MSB backfills (i.e. M5B5) is higher than that of OPC-based backfills (i.e. C5B5 and CS5B5) after being exposed to 10 wet-dry cycles. This may be attributed to the fact that the C-S-H gels formed in GGBS-MgO have a lower Ca/Si ratio compared to those formed in OPC, leading to higher shrinkage during the drying process (Jin et al., 2014; Du et al., 2016). At the same bentonite content in MSB backfills, the increase of GGBS-MgO content has only a slight impact on the dry density (i.e. comparing MS10B10 and MS10B15 with MS5B10 and MS5B15, respectively) whereas the dry density significantly decreases as the bentonite content increases from 5% to 15% at the identical GGBS-MgO content (i.e. comparing MS5B5 with MS5B10 and MS5B15) after 10 wet-dry cycles.

4.3 pH value

Fig. 5 depicts the variations in the soil pH values with the wet-dry cycles for OPC-based and MSB backfills. It can be observed that the pH for all backfills gradually decreases with increasing wet-dry cycles. This is attributed to the leaching of alkaline substances (i.e. Ca^{2+}) from the backfills when exposed to wetting. After 10 wet-dry cycles, the pH of

OPC-based and MSB backfills are 10.9–12.3 and 9.8–10.8, respectively. At the same binder and bentonite contents, the pH values of MSB backfills are much lower than those of OPC-based backfills either before or after the wet-dry cycles. For instance, the pH values for 5% GGBS-MgO in MSB backfills (i.e. MS5B5 and CS5B5) are approximately 0.5–1.2 lower than those for 5% OPC-based backfills (i.e. C5B5 and CS5B5) after 10 wet-dry cycles. Increasing the bentonite content in MSB backfills reduces the pH values by 0.4 and 0.2 unit at 5% and 10% binder contents (i.e. comparing MS5B10 and MS10B10 with MS5B15 and MS10B15, respectively) after 10 wet-dry cycles. Increasing the GGBS-MgO content results in higher pH, while increasing the bentonite content decreases the pH value in the MSB mixtures.

4.4 Unconfined compressive strength

Fig. 6 shows the evolution of q_u for the OPC-based and MSB specimens. It is found that q_u values of the two types of backfill decrease with increasing wet-dry cycles. After 10 wet-dry cycles, the q_u values of the OPC-based and MSB backfills are 400–540 kPa and 180–420 kPa, respectively. The decreased q_u is attributed to the gradually dissolved Ca^{2+} from the OPC-based and MSB matrices exposed to wetting conditions (Shen et al., 2008; Du et al., 2016). As the pH decreases to below 10.8 (Fig. 5), the partial destruction of C-S-H gels in the MSB backfill matrix also leads to lower q_u when compared to OPC-based backfills (Fig. 6). For the MSB backfills, the q_u of 10% GGBS-MgO in MSB backfills (i.e. MS10B10 and MS10B15) is 2.1–2.3 times higher

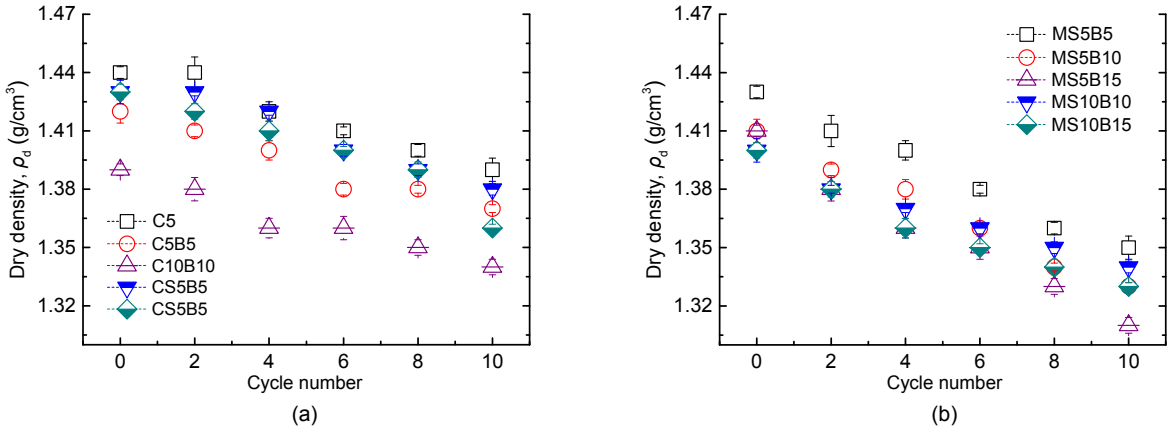

Fig. 4 Dry density values for backfills after wet-dry cycles
(a) OPC-based backfills; (b) MSB backfills

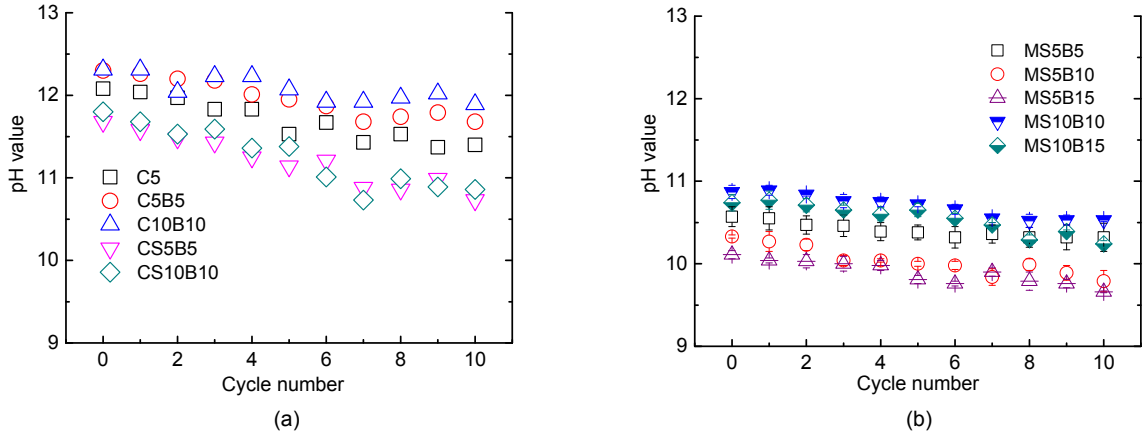

Fig. 5 Variations in pH with wet-dry cycles for OPC-based backfills (a) and MSB backfills (b)

than that of 5% GGBS-MgO (i.e. MS5B10 and MS5B15). It is also observed that increasing the bentonite content at the same binder content slightly reduces the strength of MSB mixtures, and that is consistent with the higher mass change and lower dry density shown in Fig. 2 and Fig. 4, respectively.

The strength loss (SL) and cumulative strength loss (CSL) is computed by

$$SL_i=(q_{u0}-q_{ui})/q_{u0}, \quad (2)$$

$$CSL_i=SL_0+SL_1+\ldots+SL_i, \quad (3)$$

where q_{u0} is the initial unconfined compressive strength of the specimen measured prior to the wet-dry cycles, and q_{ui} is the mass unconfined compressive strength of the sample measured immediately after the ith wet-dry cycle.

It can be observed that the CSL for 5% GGBS-MgO backfills (i.e. MS5B10 and MS5B15) is 35%–47% higher than that of 10% GGBS-MgO (i.e. MS10B10 and MS10B15) as shown in Fig. 7. Furthermore, CSL decreases by 2.7% and 6.4% for 5% and 10% GGBS-MgO in MSB backfills, respectively, as the bentonite increases from 10% to 15%. Thus, the impact of wet-dry cycles on MSB backfills is greater than that on OPC-based backfills. This phenomenon might be attributed to: (1) a lower Ca/Si ratio of C-S-H in MSB backfills as compared to that formed in the OPC-based backfills, which is more prone to shrinkage under the drying process, resulting in micro-cracking of the matrix (Jin et al., 2014) and (2) a larger amount of uncombined water remaining in the MSB backfills due to the better preserved bentonite swelling/shrinkage behavior (Wu et al., 2019), which is prone to evaporation and leads to substantial shrinkage cracking upon drying, resulting in greater strength loss.

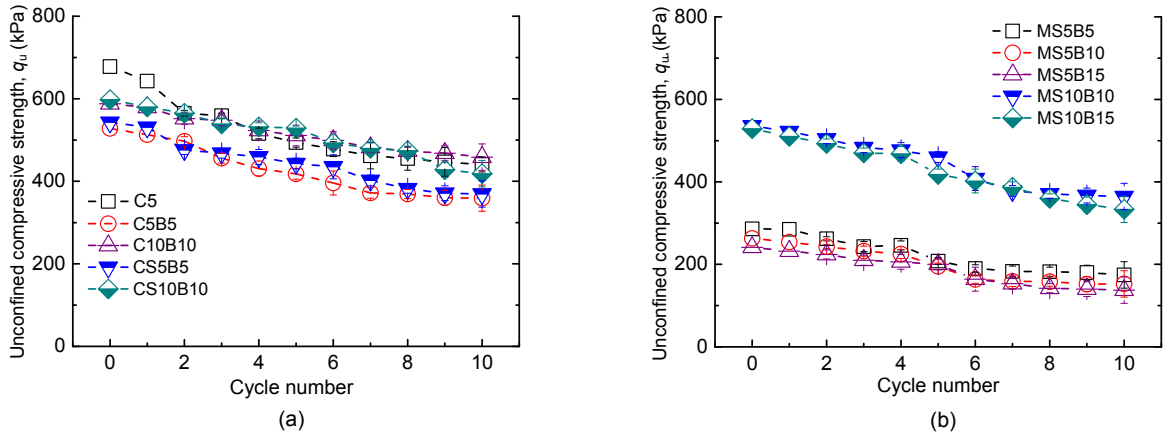

Fig. 6 Effect of wet-dry cycles on q_u for OPC-based backfills (a) and MSB backfills (b)

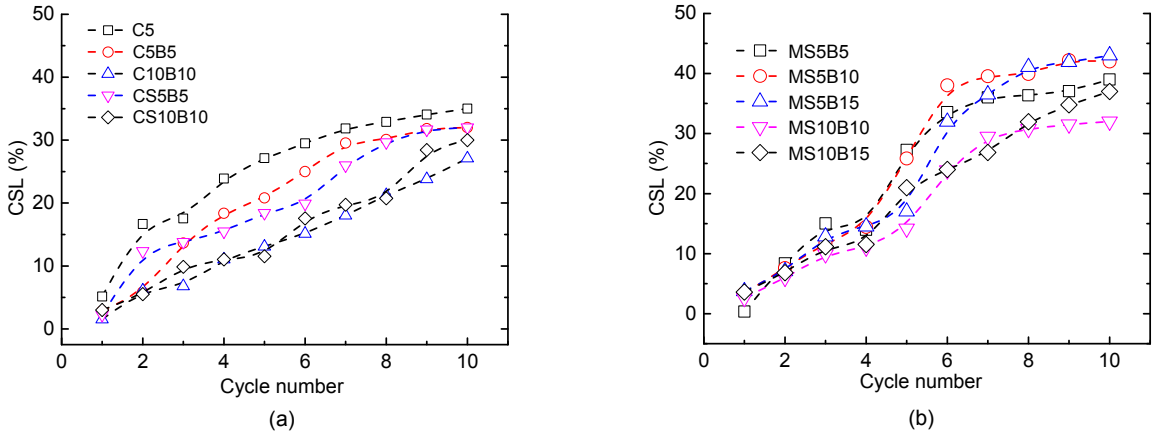

Fig. 7 Effect of wet-dry cycles on cumulative strength loss for OPC-based backfills (a) and MSB backfills (b)

4.5 Pore size distribution

To investigate the evolution in pore profiles of MSB backfills with respect to wet-dry cycles, MIP tests are conducted. Fig. 8a shows the cumulative pore volumes of the MSB backfills after 10 wet-dry cycles. At the same bentonite content, the cumulative pore volumes of MS5B10 and MS5B15 are found to decrease by 12% and 2% as compared with MS10B10 and MS10B15. At 5% GGBS-MgO content, increasing the bentonite content from 5% to 10% and 15% increases the cumulative pore volume by 4.6% and 7.9%, respectively. The results for the pore profiles are consistent with the observed trends for q_u and mass change as shown in Fig. 6b and Fig. 2b, respectively.

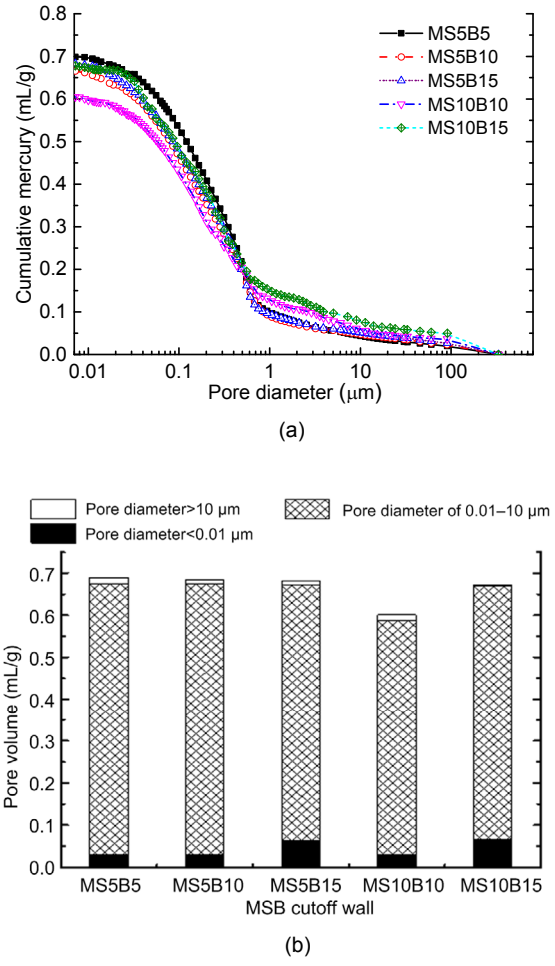

Fig. 8 Cumulative pore volume (a) and pore volume percentage (b) of MSB backfills after 90 d standard curing and subjected to 10 wet-dry cycles

Fig. 8b shows the volumes of the pores in different size ranges: <0.01 μm (intra-aggregate), 0.01–10 μm (inter-aggregate), and >10 μm (air pores) respectively. This classification of pore sizes is suggested by Horpibulsuk et al. (2010) and Xia et al. (2019a, 2019b) for the OPC stabilized silty clay. Regardless of the binder content, the proportions of air pores and inter-aggregate pores decrease but intra-aggregate pores increase as the bentonite content increases from 5% to 15%. At the same bentonite content, increasing the binder content decreases the proportions of pores in each category (i.e. comparing MS5B10 and MS10B10 with MS5B15 and MS10B15). As reported in previous studies (Collins and Sanjayan, 2000; Du et al., 2014, 2016), a larger volume of inter-aggregate pores can lead to higher drying-initiated capillary tension forces and greater shrinkage potential in the matrix. Thus, the MS10B10 mixture shows the highest q_u and the least mass change among all the MSB backfills as shown in Fig. 6 and Fig. 2, respectively.

4.6 X-ray diffraction

XRD tests were conducted on the MSB specimens before and after 10 wet-dry cycles to investigate the evolution of the phase assemblage in the mixtures as presented in Figs. 9a and 9b.

The characteristic peaks of hydrotalcite ($Mg_6Al_2(OH)_{16}CO_3{\cdot}4H_2O$)-like phases (Ht) were found at 2θ≈12.5° and 24.0°, agreeing well with previous findings (Jin and Al-Tabbaa, 2014a). In addition, two broad peaks ascribed to C-S-H were detected at 2θ≈23.0°, 30.0°, 31.6°, and 37.5°, and were the results of the reaction between released silicate species and Ca from GGBS (Jin and Al-Tabbaa, 2014a; Jin et al., 2014; Wu et al., 2019). The C-S-H gels and hydrotalcite can improve the strength and hydraulic performance in MSB cutoff wall applications. Further, hydrotalcite has contaminants (e.g. lead and zinc) with a high capacity for adsorption and which therefore can enhance the chemical compatibility of the backfills exposed to contaminated underground conditions. The higher intensity of Ht and C-S-H are observed in 10% GGBS-MgO (i.e. MS10B10 and MS10B15) as compared with 5% GGBS-MgO (i.e. MS5B5, MS5B10, and MS10B15), and result in higher q_u (Fig. 6) and lower mass change (Fig. 2). The characteristic peak of quartz (SiO_2) has

been detected at $2\theta\approx21.6°$ in the local clayey sand. The characteristic peaks of calcium hydroxide ($Ca(OH)_2$) have been detected at $2\theta\approx19.0°$, 34.5°, and 46.5°, from the leaching of Ca^{2+} from GGBS and C-S-H. The leaching of Ca^{2+} will lead to the decrease of pH value as illustrated in Fig. 5. Nesquehonite ($MgCO_3{\cdot}3H_2O$) is found in the backfills after 10 wet-dry cycles, as the peaks at $2\theta\approx14.2°$ and 41.0° agree with those reported by Wu et al. (2018b) and Ruan et al. (2019). It is formed by the dissolved Mg^{2+} from the MSB backfills and dissolved CO_2 from the atmosphere. Similarly the leached Ca^{2+} from the GGBS and C-S-H may react with dissolved atmospheric CO_2 to form calcite. Nevertheless, the strongest calcite peak ($2\theta\approx30.0°$) overlaps with that of C-S-H, which prevents its identification via XRD in this study.

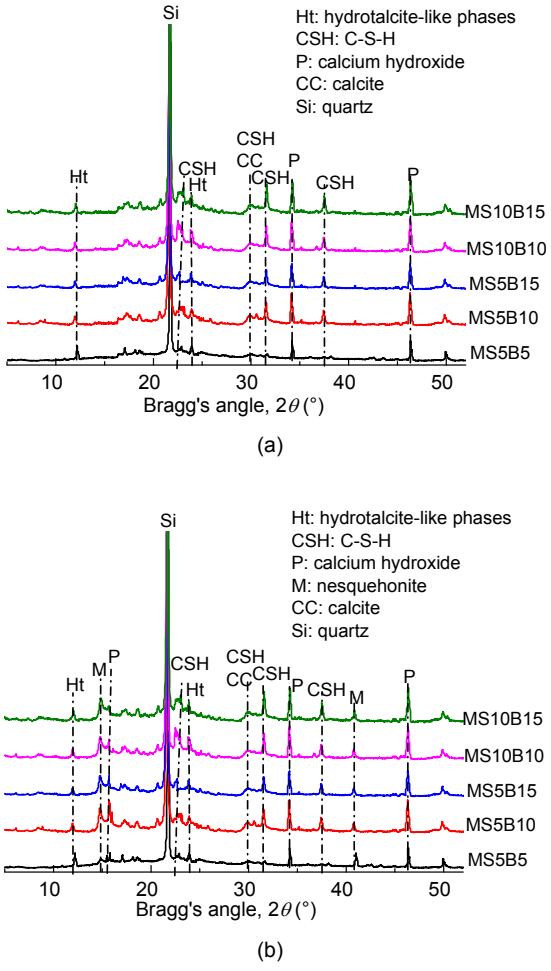

Fig. 9 X-ray diffractograms of the 90-d cured MSB backfills before (a) and after (b) wet-dry cycles

5 Limitations of current study

This study reveals that the MSB mixture is more sensitive to a fluctuating groundwater condition than OPC-based backfills. This might be attributed to the hydration products (C-S-H with a lower Ca/Si ratio) and microstructure (refined pores) formed in alkali-activated GGBS paste as compared to OPC-based backfills (Du et al., 2015). Nevertheless, the unconfined compressive strength values of MSB mixtures are still above the commonly adopted design limits ($q_u\geq100$ kPa) after 10 wet-dry cycles. The much lower pH values of pore water in MSB mixtures have much weaker impact on the chemical stability of montmorillonite in bentonite as compared to OPC-based backfills (Wu et al., 2019). In addition, the use of a large amount of industrial waste gives the MSB mixture better sustainability than the OPC-based backfills.

Admittedly, for a full understanding of the long-term durability of the MSB backfills after wet-dry cycles, the wet-dry aging could be correlated with real-time for a quantitative simulation (Shen et al., 2018, 2019). Further investigations are warranted to elucidate the change of hydraulic conductivity, hydration products, and microstructures of the backfills under the various extreme environmental stresses that might be encountered in the field.

6 Conclusions

A comprehensive laboratory testing program was conducted to reveal the effects of wet-dry cycles on the properties of MSB backfills and the following conclusions can be drawn:

1. The mass change of OPC-based and MSB backfills increased with respect to the wet-dry cycles. The MSB backfills exhibited 1.1%–2.1% higher mass change than OPC-based ones after 10 wet-dry cycles. Increasing the GGBS-MgO content reduced 9.0%–11% mass change but increasing the bentonite content increased mass change in MSB backfills. The threshold cycle numbers for spalling and macro-cracks occurring in MSB backfills were found to be in the 4th–6th cycles.

2. The dry density and pH of OPC-based and MSB backfills gradually decreased with increasing wet-dry cycles. For the identical binder (OPC and GGBS-MgO) and bentonite contents, the mass change of MSB backfills was higher than that in OPC-based backfills, while the pH was much lower.

3. The unconfined compressive strength of OPC-based and MSB backfills decreased with increasing wet-dry cycles. The strength values of the MSB backfills with 10% GGBS-MgO were 2.1–2.3 times higher than those with 5% GGBS-MgO, while increasing the bentonite content slightly reduced the strength. The cumulative strength loss of MSB backfills was more notable than that for OPC-based backfills.

4. Increasing the GGBS-MgO content from 5% to 10% reduces the cumulative pore volume by 2%–12%, while increasing the bentonite content from 5% to 15% increases the cumulative pore volume by 4.6%–7.9%.

5. The hydrotalcite-like phases and C-S-H were found to be the primary hydration products in the MSB backfills both before and after the wet-dry cycles. The wet-dry cycles accelerated the leaching of earth alkali ions, which react with the dissolved CO_2 from the atmosphere to form calcite ($CaCO_3$) and nesquehonite ($MgCO_3 \cdot 3H_2O$) in MSB mixtures.

Contributors

Hao-liang WU conducted all experiments and processed the corresponding data. Hao-liang WU wrote the first draft of the manuscript. Fei JIN and Yan-jun DU helped to organize the manuscript. Yan-jun DU designed the research. Hao-liang WU, Fei JIN, and Yan-jun DU revised and edited the final version.

Conflict of interest

Hao-liang WU, Fei JIN, and Yan-jun DU declare that they have no conflict of interest.

References

Arulrajah A, Kua TA, Suksiripattanapong C, et al., 2017a. Compressive strength and microstructural properties of spent coffee grounds-bagasse ash based geopolymers with slag supplements. *Journal of Cleaner Production*, 162:1491-1501. https://doi.org/10.1016/j.jclepro.2017.06.171

Arulrajah A, Kua TA, Horpibulsuk S, et al., 2017b. Recycled glass as a supplementary filler material in spent coffee grounds geopolymers. *Construction and Building Materials*, 151:18-27. https://doi.org/10.1016/j.conbuildmat.2017.06.050

ASTM, 2008. Standard Test Method for Unconfined Compressive Strength Index of Chemical-grouted Soils, ASTM D4219-08. National Standards of USA. https://doi.org/10.1520/D4219-08

ASTM, 2010a. Standard Test Methods for Laboratory Determination of Water (Moisture) Content of Soil and Rock by Mass, ASTM D2216-2010. National Standards of USA.

ASTM, 2010b. Standard Test Methods for Liquid Limit, Plastic Limit, and Plasticity Index of Soils, ASTM D4318. National Standards of USA.

ASTM, 2010c. Standard Test Method for Determination of Pore Volume and Pore Volume Distribution of Soil and Rock by Mercury Intrusion Porosimetry, ASTM D4404-10. National Standards of USA. https://doi.org/10.1520/D4404-10

ASTM, 2010d. Standard Test Method for Measuring the Exchange Complex and Cation Exchange Capacity of Inorganic Fine-grained Soils, ASTM D7503. National Standards of USA.

ASTM, 2014. Standard Test Methods for Specific Gravity of Soil Solids by Water Pycnometer, ASTM D854-14. National Standards of USA. https://doi.org/10.1520/D0854-14

ASTM, 2017. Standard Practice for Classification of Soils for Engineering Purposes (Unified Soil Classification System), ASTM D2487-17. National Standards of USA. https://doi.org/10.1520/D2487-17

ASTM, 2018a. Standard Test Methods for pH of Soils, ASTM D4972-18. National Standards of USA. https://doi.org/10.1520/D4972-18

ASTM, 2018b. Standard Test Methods for Laboratory Determination of Density (Unit Weight) of Soil Specimens, ASTM D7263-09(2018)e2. National Standards of USA. https://doi.org/10.1520/D7263-09R18E02

Benhelal E, Zahedi G, Shamsaei E, et al., 2013. Global strategies and potentials to curb CO_2 emissions in cement industry. *Journal of Cleaner Production*, 51:142-161. https://doi.org/10.1016/j.jclepro.2012.10.049

Cerato AB, Lutenegger AJ, 2002. Determination of surface area of fine-grained soils by the ethylene glycol monoethyl ether (EGME) method. *Geotechnical Testing Journal*, 25(3):315-321. https://doi.org/10.1520/GTJ11087J

Collins F, Sanjayan JG, 2000. Effect of pore size distribution on drying shrinking of alkali-activated slag concrete. *Cement and Concrete Research*, 30(9):1401-1406. https://doi.org/10.1016/s0008-8846(00)00327-6

Du YJ, Jiang NJ, Liu SY, et al., 2014. Engineering properties and microstructural characteristics of cement-stabilized zinc-contaminated kaolin. *Canadian Geotechnical Journal*, 51(3):289-302.

https://doi.org/10.1139/cgj-2013-0177

Du YJ, Fan RD, Liu SY, et al., 2015. Workability, compressibility and hydraulic conductivity of zeolite-amended clayey soil/calcium-bentonite backfills for slurry-trench cutoff walls. *Engineering Geology*, 195:258-268. https://doi.org/10.1016/j.enggeo.2015.06.020

Du YJ, Bo YL, Jin F, et al., 2016. Durability of reactive magnesia-activated slag-stabilized low plasticity clay subjected to drying–wetting cycle. *European Journal of Environmental and Civil Engineering*, 20(2):215-230. https://doi.org/10.1080/19648189.2015.1030088

Du YJ, Wu J, Bo YL, et al., 2019. Effects of acid rain on physical, mechanical and chemical properties of GGBS-MgO-solidified/stabilized Pb-contaminated clayey soil. *Acta Geotechnica*, in press. https://doi.org/10.1007/s11440-019-00793-y

Evans JC, 1991. Geotechnics of hazardous waste control systems. *In*: Fang HY (Ed.), Foundation Engineering Handbook, 2nd Edition. Springer, Boston, USA, p.750-777. https://doi.org/10.1007/978-1-4757-5271-7_20

Horpibulsuk S, Rachan R, Chinkulkijniwat A, et al., 2010. Analysis of strength development in cement-stabilized silty clay from microstructural considerations. *Construction and Building Materials*, 24(10):2011-2021. https://doi.org/10.1016/j.conbuildmat.2010.03.011

ICE (Institution of Civil Engineers), 1999. Specification for the Construction of Slurry Trench Cut-off Walls: As Barriers to Pollution Migration. Thomas Telford, London, UK. https://doi.org/10.1680/sftcostcw.26254

Jefferis S, 2012. Cement-bentonite slurry systems. *In*: Johnsen LF, Bruce DA, Byle MJ (Eds.), Grouting and Deep Mixing. ASCE, Reston, USA, p.1-24. https://doi.org/10.1061/9780784412350.0001

Jin F, Al-Tabbaa A, 2014a. Characterisation of different commercial reactive magnesia. *Advances in Cement Research*, 26(2):101-113. https://doi.org/10.1680/adcr.13.00004

Jin F, Al-Tabbaa A, 2014b. Evaluation of novel reactive MgO activated slag binder for the immobilisation of lead and zinc. *Chemosphere*, 117:285-294. https://doi.org/10.1016/j.chemosphere.2014.07.027

Jin F, Gu K, Al-Tabbaa A, 2014. Strength and drying shrinkage of reactive MgO modified alkali-activated slag paste. *Construction and Building Materials*, 51:395-404. https://doi.org/10.1016/j.conbuildmat.2013.10.081

Jin F, Gu K, Al-Tabbaa A, 2015. Strength and hydration properties of reactive MgO-activated ground granulated blastfurnace slag paste. *Cement and Concrete Composites*, 57:8-16. https://doi.org/10.1016/j.cemconcomp.2014.10.007

Joshi K, Soga K, Ng MYA, et al., 2008. Durability study of eleven years old cement-bentonite cut-off wall material. *In*: Khire MV, Alshawabkeh AN, Reddy KR (Eds.), GeoCongress 2008: Geotechnics of Waste Management and Remediation. ASCE, New Orleans, USA, p.620-627. https://doi.org/10.1061/40970(309)78

Joshi K, Kechavarzi C, Sutherland K, et al., 2010. Laboratory and in situ tests for long-term hydraulic conductivity of a cement-bentonite cutoff wall. *Journal of Geotechnical and Geoenvironmental Engineering*, 136(4):562-572. https://doi.org/10.1061/(asce)gt.1943-5606.0000248

Kamon M, Nontananandh S, Katsumi T, 1993. Utilization of stainless-steel slag by cement hardening. *Soils and Foundations*, 33(3):118-129. https://doi.org/10.3208/sandf1972.33.3_118

Lam C, Jefferis SA, 2017. Polymer Support Fluids in Civil Engineering. ICE Publishing, London, UK. https://doi.org/10.1680/psfce.57869

Li YC, Tong X, Chen Y, et al., 2018. Non-monotonic piezocone dissipation curves of backfills in a soil-bentonite slurry trench cutoff wall. *Journal of Zhejiang University-SCIENCE A (Applied Physics & Engineering)*, 19(4):277-288. https://doi.org/10.1631/jzus.A1700097

Malusis MA, Yeom S, Evans JC, 2011. Hydraulic conductivity of model soil–bentonite backfills subjected to wet–dry cycling. *Canadian Geotechnical Journal*, 48(8):1198-1211. https://doi.org/10.1139/t11-028

Nahlawi H, Kodikara JK, 2006. Laboratory experiments on desiccation cracking of thin soil layers. *Geotechnical and Geological Engineering*, 24(6):1641-1664. https://doi.org/10.1007/s10706-005-4894-4

National Research Council, 2007. Assessment of the Performance of Engineered Waste Containment Barriers. The National Academies Press, Washington, USA. https://doi.org/10.17226/11930

Opdyke SM, Evans JC, 2005. Slag-cement-bentonite slurry walls. *Journal of Geotechnical and Geoenvironmental Engineering*, 131(6):673-681. https://doi.org/10.1061/(asce)1090-0241(2005)131:6(673)

Ross RR, Beljin MS, 1998. Evaluation of containment systems using hydraulic head data. *Journal of Environmental Engineering*, 124(6):575-578. https://doi.org/10.1061/(asce)0733-9372(1998)124:6(575)

Rowe RK, Bostwick LE, Take WA, 2011. Effect of GCL properties on shrinkage when subjected to wet-dry cycles. *Journal of Geotechnical and Geoenvironmental Engineering*, 137(11):1019-1027. https://doi.org/10.1061/(asce)gt.1943-5606.0000522

Ruan SQ, Qiu JS, Weng YW, et al., 2019. The use of microbial induced carbonate precipitation in healing cracks within reactive magnesia cement-based blends. *Cement and Concrete Research*, 115:176-188. https://doi.org/10.1016/j.cemconres.2018.10.018

Ruffing DG, Evans JC, 2014. Case study: construction and in

situ hydraulic conductivity evaluation of a deep soil-cement-bentonite cutoff wall. Proceedings of GeoCongress 2014, p.1836-1848. https://doi.org/10.1061/9780784413272.180

Ryan CR, Day SR, 2002. Soil-cement-bentonite slurry walls. *In*: O'Neill MW, Townsend FC (Eds.), Deep Foundations 2002: an International Perspective on Theory, Design, Construction, and Performance. Geotechnical Special Publication, New York, USA, p.713-727. https://doi.org/10.1061/40601(256)51

Shand MA, 2006. The Chemistry and Technology of Magnesia. John Wiley & Sons, Hoboken, USA.

Shen SL, Han J, Du YJ, 2008. Deep mixing induced property changes in surrounding sensitive marine clays. *Journal of Geotechnical and Geoenvironmental Engineering*, 134(6):845-854. https://doi.org/10.1061/(asce)1090-0241(2008)134:6(845)

Shen ZT, Hou DY, Xu WD, et al., 2018. Assessing long-term stability of cadmium and lead in a soil washing residue amended with MgO-based binders using quantitative accelerated ageing. *Science of the Total Environment*, 643:1571-1578. https://doi.org/10.1016/j.scitotenv.2018.06.321

Shen ZT, Pan SZ, Hou DY, et al., 2019. Temporal effect of MgO reactivity on the stabilization of lead contaminated soil. *Environment International*, 131:104990. https://doi.org/10.1016/j.envint.2019.104990

Soga K, Joshi K, Evans JC, 2013. Cement bentonite cutoff walls for polluted sites. Proceedings of Coupled Phenomena in Environmental Geotechnics, p.149-165. https://doi.org/10.1201/b15004-15

Tang CS, Shi B, Liu C, et al., 2011. Experimental characterization of shrinkage and desiccation cracking in thin clay layer. *Applied Clay Science*, 52(1-2):69-77. https://doi.org/10.1016/j.clay.2011.01.032

Wang F, Jin F, Shen ZT, et al., 2016. Three-year performance of in-situ mass stabilised contaminated site soils using MgO-bearing binders. *Journal of Hazardous Materials*, 318:302-307. https://doi.org/10.1016/j.jhazmat.2016.07.018

Wu HL, Du YJ, Wang F, et al., 2016. Workability and strength characteristics of alkali-activated slag-bentonite backfills for vertical slurry cutoff wall. *Journal of Southeast University (Natural Science Edition)*, 46(S1):25-30 (in Chinese).

Wu HL, Jin F, Bo YL, et al., 2018a. Leaching and microstructural properties of lead contaminated kaolin stabilized by GGBS-MgO in semi-dynamic leaching tests. *Construction and Building Materials*, 172:626-634. https://doi.org/10.1016/j.conbuildmat.2018.03.164

Wu HL, Zhang D, Ellis BR, et al., 2018b. Development of reactive MgO-based engineered cementitious composite (ECC) through accelerated carbonation curing. *Construction and Building Materials*, 191:23-31. https://doi.org/10.1016/j.conbuildmat.2018.09.196

Wu HL, Jin F, Ni J, et al., 2019. Engineering properties of vertical cutoff walls consisting of reactive magnesia-activated slag and bentonite: workability, strength, and hydraulic conductivity. *Journal of Materials in Civil Engineering*, 31(11):04019263. https://doi.org/10.1061/(asce)mt.1943-5533.0002908

Xia WY, Du YJ, Li FS, et al., 2019a. Field evaluation of a new hydroxyapatite based binder for ex-situ solidification/stabilization of a heavy metal contaminated site soil around a Pb-Zn smelter. *Construction and Building Materials*, 210:278-288. https://doi.org/10.1016/j.conbuildmat.2019.03.195

Xia WY, Du YJ, Li FS, et al., 2019b. In-situ solidification/stabilization of heavy metals contaminated site soil using a dry jet mixing method and new hydroxyapatite based binder. *Journal of Hazardous Materials*, 369:353-361. https://doi.org/10.1016/j.jhazmat.2019.02.031

Yang YL, Reddy KR, Du YJ, et al., 2018a. Short-term hydraulic conductivity and consolidation properties of soil-bentonite backfills exposed to CCR-impacted groundwater. *Journal of Geotechnical and Geoenvironmental Engineering*, 144(6):04018025. https://doi.org/10.1061/(asce)gt.1943-5606.0001877

Yang YL, Reddy KR, Du YJ, et al., 2018b. Sodium hexametaphosphate (SHMP)-amended calcium bentonite for slurry trench cutoff walls: workability and microstructure characteristics. *Canadian Geotechnical Journal*, 55(4):528-537. https://doi.org/10.1139/cgj-2017-0291

Yang YL, Reddy KR, Du YJ, et al., 2019. Retention of Pb and Cr(VI) onto slurry trench vertical cutoff wall backfill containing phosphate dispersant amended Ca-bentonite. *Applied Clay Science*, 168:355-365. https://doi.org/10.1016/j.clay.2018.11.023

Yi YL, Liska M, Al-Tabbaa A, 2014. Properties of two model soils stabilized with different blends and contents of GGBS, MgO, lime, and PC. *Journal of Materials in Civil Engineering*, 26(2):267-274. https://doi.org/10.1061/(asce)mt.1943-5533.0000806

Zhang WB, Rao WB, Li L, et al., 2019. Compressibility and hydraulic conductivity of sand-attapulgite cut-off wall backfills. *Journal of Zhejiang University-SCIENCE A (Applied Physics & Engineering)*, 20(3):218-228. https://doi.org/10.1631/jzus.a1800548

中文概要

题　目：干湿循环作用下氧化镁激发矿渣-膨润土竖向隔离墙耐久特性研究

目　的： 1. 研究干湿循环作用下氧化镁激发矿渣-膨润土

（MSB）竖向隔离墙的耐久特性。2. 探讨干湿循环过程中循环级数对隔离墙的质量变化、干密度、pH 值、无侧限抗压强度、孔隙结构和微观产物等的影响，并探究 MSB 的服役性能。

创新点： 1. 通过干湿循环作用，揭示新型 MSB 隔离墙与传统水泥基（OPC）隔离墙的耐久性差异；2. 通过微观分析，成功测定新型 MSB 隔离墙干湿循环后形成的水化产物。

方　法： 1. 通过宏观实验分析，在干湿循环作用下比较 MSB 隔离墙和 OPC 隔离墙的质量、干密度、pH 值和无侧限抗压强度等参数的变化情况（图 2 和 4~6）；2. 通过微观分析，研究 MSB 隔离墙中氧化镁激发高炉矿渣（GGBS-MgO）和膨润土的掺量对空隙结构的影响（图 8），并探讨干湿循环作用如何影响碳酸钙和碳酸镁等水化产物的形成（图 9）。

结　论： 1. MSB 隔离墙的质量损失比 OPC 隔离墙高 1.1%~2.1%；2. MSB 和 OPC 隔离墙的干密度和 pH 值均随干湿循环级数的增长而减小；3. MSB 和 OPC 隔离墙的无侧限抗压强度随干湿循环级数的增长而降低；4. 增加 GGBS-MgO 的掺量可减少 2%~12%的累计进汞量，而增加膨润土的掺量会增加 4.6%~7.9%的进汞量；5. 干湿循环可加速碳酸钙和碳酸镁等水化产物的形成。

关键词： 竖向隔离墙；氧化镁激发矿渣；耐久特性；干湿循环；碳化